Nanoscale Perturbations of Room Temperature Ionic Liquid Structure at Charged and Uncharged Interfaces

ARTICLE *in* ACS NANO · OCTOBER 2012

Impact Factor: 12.88 · DOI: 10.1021/nn303355b · Source: PubMed

12 AUTHORS, INCLUDING:

Guang Feng
Huazhong University of Science and Technol…
47 PUBLICATIONS **775** CITATIONS
SEE PROFILE

Peter T Cummings
Vanderbilt University
512 PUBLICATIONS **11,498** CITATIONS
SEE PROFILE

Pasquale F Fulvio
University of Puerto Rico at Rio Piedras
70 PUBLICATIONS **2,136** CITATIONS
SEE PROFILE

Yury Gogotsi
Drexel University
625 PUBLICATIONS **25,521** CITATIONS
SEE PROFILE

Nanoscale Perturbations of Room Temperature Ionic Liquid Structure at Charged and Uncharged Interfaces

Hua Zhou,[†,#,*] Michael Rouha,[‡] Guang Feng,[‡] Sang Soo Lee,[†] Hugh Docherty,[‡] Paul Fenter,[†,*] Peter T. Cummings,[‡,§] Pasquale F. Fulvio,[⊥] Sheng Dai,[⊥] John McDonough,[¶] Volker Presser,[¶,▽] and Yury Gogotsi[¶]

[†]Chemical Science and Engineering Division, Argonne National Laboratory, Argonne, Illinois 60439, United States, [‡]Department of Chemical and Biomolecular Engineering, Vanderbilt University, Nashville, Tennessee 37235, United States, [§]Center for Nanophase Materials and [⊥]Chemical Science Division, Oak Ridge National Laboratory, Oak Ridge, Tennessee 37831, United States, and [¶]Department of Materials Science and Engineering & A.J. Drexel Nanotechnology Institute, Drexel University, Philadelphia, Pennsylvania 19104, United States. [#]Present address: Advanced Photon Source, Argonne National Laboratory, Argonne, IL 60439. [▽]Present address: INM Leibniz-Institut für Neue Materialien gGmbH, Campus D2 2, 66123 Saarbrücken, Germany.

ABSTRACT The nanoscale interactions of room temperature ionic liquids (RTILs) at uncharged (graphene) and charged (muscovite mica) solid surfaces were evaluated with high resolution X-ray interface scattering and fully atomistic molecular dynamics simulations. At uncharged graphene surfaces, the imidazolium-based RTIL ([bmim$^+$][Tf_2N^-]) exhibits a mixed cation/anion layering with a strong interfacial densification of the first RTIL layer. The first layer density observed *via* experiment is larger than that predicted by simulation and the apparent discrepancy can be understood with the inclusion of, dominantly, image charge and π-stacking interactions between the RTIL and the graphene sheet. In contrast, the RTIL structure adjacent to the charged mica surface exhibits an alternating cation–anion layering extending 3.5 nm into the bulk fluid. The associated charge density profile demonstrates a pronounced charge overscreening (*i.e.*, excess first-layer counterions with respect to the adjacent surface charge), highlighting the critical role of charge-induced nanoscale correlations of the RTIL. These observations confirm key aspects of a predicted electric double layer structure from an analytical Landau–Ginzburg-type continuum theory incorporating ion correlation effects, and provide a new baseline for understanding the fundamental nanoscale response of RTILs at charged interfaces.

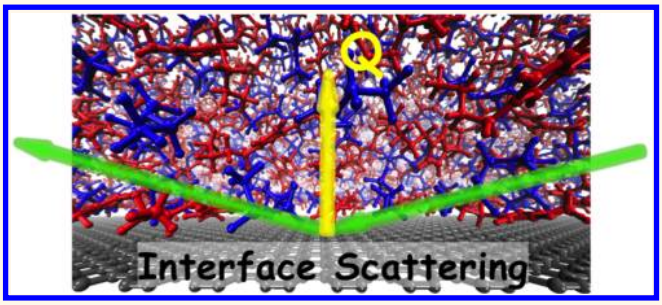

KEYWORDS: Room temperature ionic liquid · densification · epitaxial graphene · mica · charge overscreening · interfacial structure · X-ray reflectivity

Room temperature ionic liquids (RTILs) are attractive for many applications due to their selective and wide electrochemical stability windows, high ion conductivities, and low environmental impacts.[1−3] These properties offer great potential for their development as advanced solvent-free electrolytes for electrochemical energy storage systems, including batteries/fuel cells (redox reactions) and electrochemical double-layer capacitors (non-Faradic reactions).[1,2,4] A missing ingredient for developing these applications is a deep and robust understanding of the intrinsic, molecular-scale interactions of RTILs with carbon-based electrodes, which control the properties of these interfaces and influence the resulting electrochemical performance.[5] Extensive computational studies of RTILs at graphitic carbon surfaces (such as graphene/graphite,[6−9] carbon nanotubes,[10−12] and onion-like carbon[13]) have explored the behavior of RTILs in energy storage and conversion.[14−16] Yet, there is very little that is known experimentally about the molecular-scale behavior of RTILs at carbon surfaces through *in situ* observations (and very few results for RTILs at any solid–liquid interface[17,18]) that can be used to validate these predictions. This is in part due to the highly textured and complex morphologies of most graphitic carbons.[19−21] The development of atomically flat two-dimensional epitaxial graphene (EG) grown on single-crystal silicon carbide (SiC)[22,23] in combination with interface X-ray scattering opens a new route to understanding RTIL-carbon interactions at ambient conditions with a truly molecular-scale perspective, as

* Address correspondence to hzhou@anl.gov, fenter@anl.gov.

Received for review July 26, 2012 and accepted October 23, 2012.

Published online October 23, 2012
10.1021/nn303355b

has recently been demonstrated for the water/graphene interface.[24]

The behavior of RTILs is also broadly interesting due to their potentially complex interactions with solids, due to competition between van der Waals, dipole, hydrogen bonding, and Coulomb interactions.[25,26] An understanding of the electrochemical double layer structure of ionic liquids is complicated by the strong ion−ion correlations in RTILs. A conceptual model is needed that goes far beyond the classical Gouy−Chapman−Stern−Helmholtz concept of the electrical double layer,[27] which has only been successful in describing aqueous solutions primarily within the dilute ion limit. Various mean-field theories that take into account the crowding of finite-sized ions have been developed for highly concentrated electrolyte solutions, but have not yet incorporated the short-range Coulomb correlations that are needed for RTIL systems.[27−29] Most recently, a simple phenomenological continuum theory utilizing Landau−Ginzburg-like functional for the total free energy and incorporating ion correlation effects was developed by Bazant *et al*. to predict analytically the interfacial structures of generic ionic liquids at a charged surface.[30] So far, this model has not been tested experimentally due to lack of molecular-scale resolution of RTILs at charged interfaces. The work by Mezger *et al*. inferred the formation of alternating cation−anion double layering of imidazolium-based RTILs at a charged sapphire surface using X-ray reflectivity in the Fresnel reflectivity regime.[17,18] This work, however, had two substantial limitations: the spatial resolution of the X-ray data was limited to 4.5 Å so the interfacial RTIL structure was not fully resolved, and the origin of the surface charge was not characterized since it was assumed to be induced by the X-ray beam itself. Consequently, quantitative comparison of the molecular and/or charge distribution profiles with computational/analytical methods to test the validity and applicability of various models remains unavailable.

In this paper, we present the first molecular-scale study of RTIL distributions at solid surfaces through an integrated theory, modeling, simulation, and experiment approach. By combining high resolution X-ray reflectivity and fully atomistic molecular dynamics (MD) simulations, the intrinsic structures and interactions of an imidazolium-based RTIL [bmim$^+$][Tf$_2$N$^-$] were investigated at two surfaces with distinct surface charges, yet with similar texture and structure: the neutral semimetallic EG layers on SiC substrates, and the negatively charged muscovite mica (001) cleavage surface. In each case, high resolution scattering data can be obtained from their atomically flat surfaces. Our studies reveal a strongly enhanced interfacial densification of [bmim$^+$][Tf$_2$N$^-$] with mixed anion/cation layers at an uncharged graphene surface. In contrast, an alternating cation−anion double-layer stacking is observed adjacent to a charged mica surface with an associated charge overscreening extending 2−3 nm into solution. A quantitative analysis of charge overscreening at the charged mica interface provides a direct benchmark to test the recently proposed Landau−Ginzburg-type continuum theory incorporating ion correlation effects.[30] To our knowledge, such a quantitative comparison of molecular-level structural insights by X-ray scattering with computational/analytical approaches to study RTIL-solid interfaces has not, until now, been reported. Our observations shed new light on the electrochemistry and functionalization of graphene-based materials that utilize RTILs,[31,32] and bear significant implications for the understanding and control of RTIL−solid interactions in heterogeneous systems as diverse as thin film deposition, lubrications, and catalysis.[33−35]

RESULTS AND DISCUSSION

First, molecular layering of [bmim$^+$][Tf$_2$N$^-$] on EG was studied to understand the intrinsic RTIL structure and interactions at a carbon-electrode surface in the absence of a surface charge. Interfacial structures of [bmim$^+$][Tf$_2$N$^-$] at a graphene surface, as depicted by a snapshot obtained from our MD simulation in Figure 1A, were investigated by measuring the specular X-ray reflectivity (XR) signal. Figure 1A illustrates a schematic drawing of the XR scattering geometry in this work. Prior to the XR experiments, we carried out Raman spectroscopy to characterize the EG samples, and the measured Raman excitation bands identify the existence of graphene and the underlying 6H-SiC substrate, as shown in Figure 1(B,C). The full width at half-maximum (fwhm) of the 2D band of 58 cm^{-1} (also known as G′) at 2721 cm^{-1} is in good agreement with that predicted for bilayer graphene (BLG) based on the expected inverse linear relationship between the fwhm and the number of layers.[36] Subsequent XR analysis corroborated this layer thickness (see below). The height-derivative atomic force microscopy (AFM) image, which provides an enhanced contrast between terraces and adjacent graphene layers of a clean BLG sample (*i.e.*, in air) [Figure 1D], shows a step-terrace morphology inherited from the SiC substrate. The obtained surface topography is consistent with the structural features of graphene layers resolved from the XR analysis.

The characteristics of the EG/SiC sample used in this study were reported previously.[24] The solid substrate has a BLG film with two partial carbon layers on top of a 6 $\sqrt{3}$ × 6 $\sqrt{3}$ R30° reconstructed carbon buffer layer (G_0) commensurate with SiC,[37] as illustrated by the structural model shown in the inset of Figure 2B. X-ray reflectivity data for the [bmim$^+$][Tf$_2$N$^-$]/EG/SiC interfacial system is shown in Figure 2A. Model-dependent nonlinear least-squares fitting routines, guided by a Fienup-type phase retrieval algorithm for one-dimensional

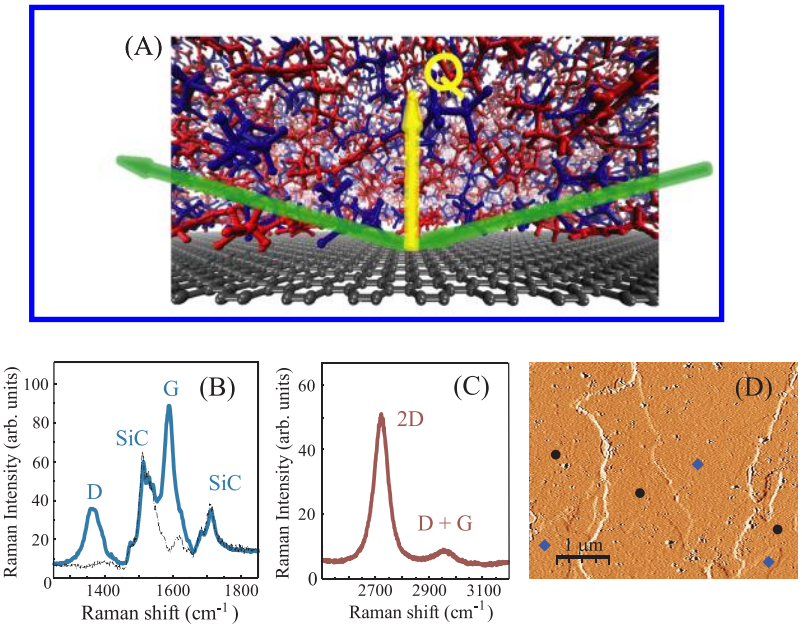

Figure 1. (A) The schematic drawing of the scattering geometry for high resolution X-ray reflectivity of epitaxial graphene on SiC interfaced with an ionic liquid. The incident and reflected X-rays indicated by the green arrows, the momentum transfer, *Q*, indicted by the vertical yellow arrow are superimposed on a snapshot of the distribution of [bmim$^+$][Tf_2N^-] molecules at the graphene surface, obtained from MD simulations (The red, blue and gray atoms/bonds represent [bmim$^+$] cations, [Tf_2N^-] anions, and graphene surface, respectively). (B and C) Raman spectra serve as a fingerprint to identify both SiC and epitaxial graphene excitation bands. The narrow solid black line in panel B represents the spectra for bare SiC substrate. (D) Height-derivative AFM image of epitaxial graphene on SiC. The solid circles represent the first graphene layer and solid diamonds for the second graphene layer with an incomplete coverage. The scale bar is 1 μm.

structure determination,[38] were used to derive the interfacial structures, in particular accounting for incomplete graphene layer coverages. From the analysis, the fraction of the surface covered by the G_n ($n > 0$) is 82% as opposed to 10% for G_0. The derived best-fit electron density profile of the BLG sample in contact with [bmim$^+$][Tf_2N^-] is shown in Figure 2B. The decrease in coverage of subsequent EG layers implies that interfacial RTIL structures are formed separately in contact with G_0, G_1, G_2, *etc*. Previous XR studies showed that the properties of G_n ($n > 0$) layers match those of intrinsic graphene (free-standing graphene), but that they are distinct from those of G_0 which behaves differently because it is strongly bound to SiC.[24] Consequently, we will focus our discussion on the RTIL structures in contact with the G_n ($n > 0$) layers, that is, the intrinsic graphene layers (The XR determined density profile above G_0 is included in the Supporting Information). In this structural model, two Gaussian electron density distributions were used to represent intrinsic RTIL structures closest to the graphene layer. The subsequent liquid structures were represented by a distorted layered liquid model used successfully in previous studies of solid/liquid and liquid/air interfacial phenomena (see Supporting Information).[39,40]

The experimentally determined RTIL structures above the intrinsic graphene layer are shown in Figure 3. The peak at the origin represents an intrinsic graphene layer (*e.g.*, G_1 or G_2). The vertical density profiles are normalized by the partial coverage of the particular EG layer which is exposed to the RTIL so that the plotted profile corresponds to the intrinsic RTIL-graphene profile. Distinct peaks of adsorbed [bmim$^+$][Tf_2N^-] are observed above the graphene layer. The density oscillations extend up to 20 Å into the bulk solution. The first adsorbed peak, with an average height of 3.20 $\pm$ 0.03 Å above graphene, exhibits a peak density that is more than three times higher than the electron density of the bulk RTIL (0.45 $e^-/Å^3$), highlighting the significant molecular layering and interfacial densification of the RTIL at the graphene surface.[41] The vertical distribution width of the peak is narrow (*i.e.*, fwhm of 0.92 $\pm$ 0.16 Å), thus indicating the presence of specific conformational arrangements of the adsorbed molecules at the surface.[41]

To gain more fundamental understanding of the interface layering of the RTIL on uncharged intrinsic graphene, we performed fully atomistic MD simulations utilizing standard semiempirical force fields for carbon and RTIL molecules. In this study, we used two sets of parameters for the interactions between carbon atoms in graphene. First we derived a set of parameters for the van-der-Waals interactions between carbon atoms and the atoms in the ionic liquids by combining the carbon−carbon interaction in the Girifalco *et al.*[42] force field with the Zhao *et al.*[43] force field for [bmim$^+$][Tf_2N^-] using Lorentz−Berthelot rules, leading to graphene-RTIL cross-interaction parameters. The primary features of the total electron density profiles obtained from the simulation using the aforementioned parameters [MD I in Figure 3A] qualitatively

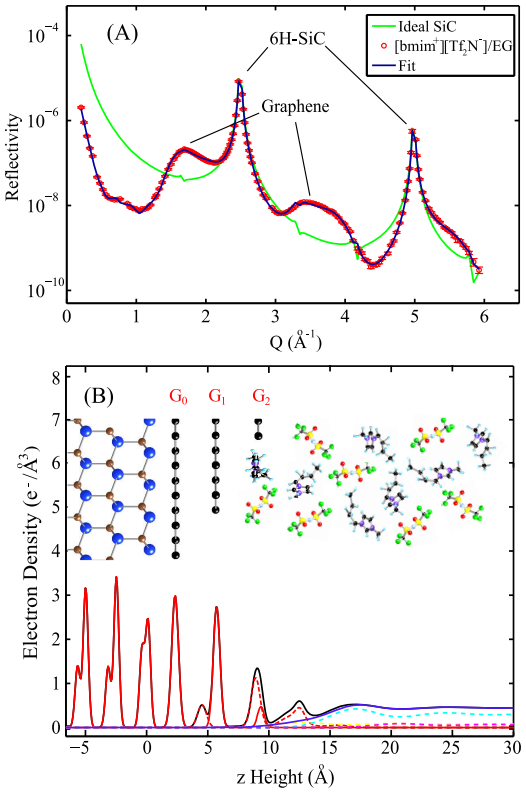

Figure 2. X-ray reflectivity data and derived total electron density profile for [bmim$^+$][Tf$_2$N$^-$] interfaced with a bilayer graphene (BLG) film on SiC. (A) XR data (circle) and the best fit, as compared with the calculated XR for an ideal SiC substrate. (B) The density profile generated from the structural model for the RTIL/EG/SiC interfacial system: (red solid line) relaxed SiC and EG layers; (red dashed line) adsorbed liquid layers above respective EG layers; (yellow (cyan, magenta) dashed line) distorted layered liquid above G_0 (G_1, G_2); (black solid line) total electron density of the RTIL; (purple shaded band) $\pm 1\sigma$ vertical uncertainties for the liquid density. (Inset) schematic drawing of the structural model: blue, Si; brown, C in SiC; black, C in graphene.

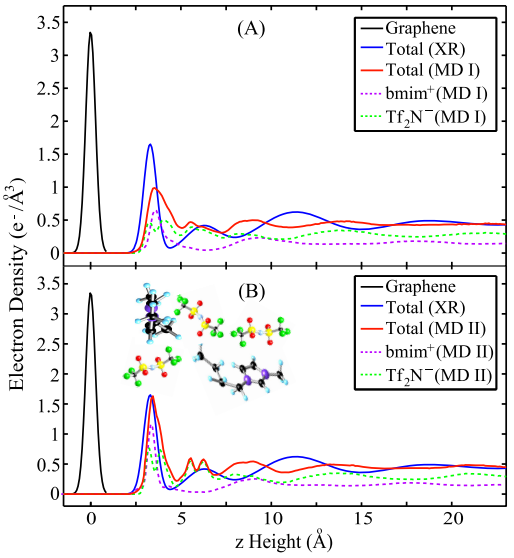

Figure 3. Interfacial RTIL structures near graphene obtained from XR data (blue solid lines), as compared to fully atomistic MD simulations (red solid line and dashed lines). (A) MD I: the simulation using graphene-IL cross-interaction parameters derived from reported force-fields for the carbon−carbon and [bmim$^+$][Tf$_2$N$^-$] interactions. (B) MD II: the simulation with a simple modification to increase the dispersion interaction strength between the surface and the liquid, after taking into account a few factors described in the text that there would probably be in reality. Inset: The schematic of the [bmim$^+$]-[Tf$_2$N$^-$] molecular distribution near the graphene layer.

resemble those obtained by XR. However, there are numerous discrepancies with respect to the XR results: the first RTIL peak shows a smaller density enhancement, with only about double that of the bulk liquid density and with a broader peak width. Also the first layer height is found at 3.56 Å above the graphene layer (0.3−0.4 Å higher that obtained by XR). These significant differences indicate that the attractive interactions between [bmim$^+$][Tf$_2$N$^-$] with graphene are significantly underestimated by MD simulations that employ a simple combination of common empirical force fields, leading to a considerably more loosely packed RTIL layer near graphene.

This quantitative disagreement could be attributed to three possible deficiencies in the force fields employed. The first is the conductive nature of the graphene sheets, which is not taken into account by the nonpolarizable interactions employed in the MD simulation. The use of nonpolarizable interactions underestimates the attraction between the liquid and the polarizable graphene sheet.[44,45] Moreover, our MD simulations together with other recent computational results[6−8] show that [bmim$^+$] cations and [Tf$_2$N$^-$] anions tend to form mixed layers, but with higher cation concentrations in the first adsorbed layer. The orientational order parameter extracted from the simulations reveals that the imidazolium rings of the first-layer cations preferentially lie down parallel to the surface plane. This provides a mechanism for the narrowing of the first RTIL layer density peak,[6−8] which was corroborated by the observed narrow density distribution of the first RTIL layer (see above) from the XR analysis. A second factor that is not directly included in the MD potentials is the potentially strong $\pi-\pi$ interactions between the imidazolium ring and the graphene basal plane which may well be a dominant factor in inducing the strong densification.[46] However, we do note that attractive interactions between atoms in the imidazolium ring and the graphene basal plane have the effect of favoring configurations in which the rings in both align in parallel, close alignment (as in $\pi-\pi$ stacking); what is absent from our forcefield is the explicit inclusion of an interaction to specifically model $\pi-\pi$ interactions. The third possible factor is associated with nanometer-sized heterogeneities observed in the bulk liquid of imidazolium-based RTILs due to micellization of the nonpolar alkyl chains separated by cation−anion pairs. This effect has been recently shown by either simulations with multiscale coarse-grained models, or X-ray scattering or high-resolution transmission electron microscopy, to be significant for

alkyl chain lengths of four or more carbon atoms (*i.e.*, starting with the butyl group).[47−49] It is reasonable to hypothesize that the accumulation of nanoaggregates in [bmim$^+$] may well be enhanced at a surface due to the potentially strong $\pi-\pi$ interactions, resulting in a higher density of cations at the surface.

To account for all of the above-mentioned factors, in principle one should employ more sophisticated methods, such as electrode charge dynamics and/or specific force fields including $\pi-\pi$ interactions,[46,50,51] thus significantly increasing the computational cost and complexity of the simulation. An alternative way, without sacrificing simplicity or speed, is to increase the dispersion interaction strength between graphene atoms and the RTIL atoms to account for those factors. This is a simple, albeit the least sophisticated, way to do this, and is essentially a simple modification of the graphene/RTIL cross interactions informed by the X-ray experiments. This modification is fully consistent with semiempirical force fields typically being derived by fitting to a combination of first principles and experimental data. By increasing the attraction between the IL and the graphene sheet by a factor of ~3 the MD results more closely resemble the experimental results. With this modified set of interaction parameters [MD II in Figure 3B], the first peak of the adsorbed RTIL layer density obtained from the modified MD simulation agrees remarkably well with the experimental observation. Other features of the density profile are also well reproduced. While the modification of the interaction strength is largely phenomenological, it illustrates that the increased attraction is needed to reproduce the behavior of the RTIL in contact with graphene, as observed by the X-ray experiments. Ideally, the change of the attraction between graphene and the RTIL should be obtained by performing *ab initio* MD simulations as compared to classical MD simulations, which would be further investigated in our future work with the collaborating computations including full information of interactions between the RTIL and solid surface.

We now address the question of how the interfacial structures and interactions of the RTIL are altered in response to the presence of a charged surface. This issue was addressed by probing the molecular layering of [bmim$^+$][Tf$_2$N$^-$] at a charged muscovite mica surface. Muscovite mica is a layer-silicate mineral that is structurally similar to graphene, but has a fixed layer charge of ~1e$^-$ /46.7 Å^2,[52] which is compensated by K$^+$ ions. Extensive studies have shown that K$^+$ desorbs readily in aqueous solutions.[39,53] Comparison of our present results with MD simulations shows that agreement is only achieved when the K$^+$ ions are removed from the surface, thus suggesting that they are displaced by the RTIL (see Supporting Information, Figure S3 and associated text). Various scanning probe microscopy studies of mica-RTIL systems have observed lateral domains suggesting a vertical layering of RTILs near the charged surface.[54−56]

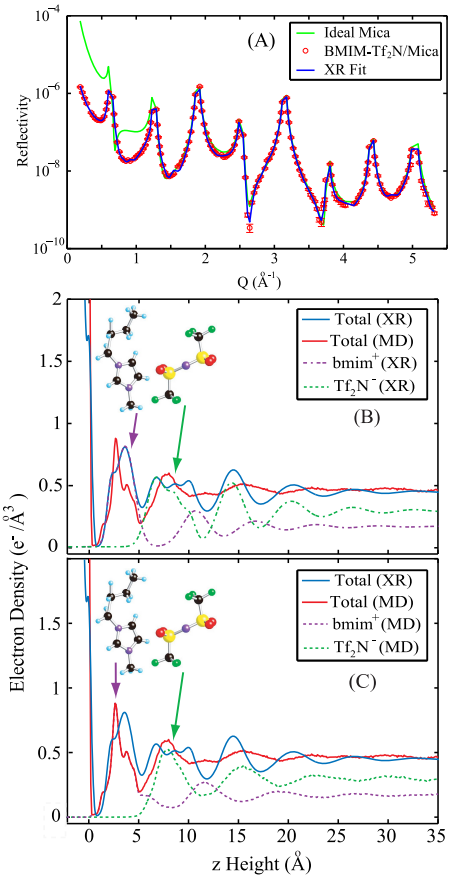

Figure 4. X-ray reflectivity data and derived total density profiles for the [bmim$^+$][Tf$_2$N$^-$]/mica interfacial system. (A) XR data and best fits, as compared with the calculated XR for an ideal mica substrate. (B−C) Interfacial RTIL structures near the charged mica surface obtained from fitting as compared to fully atomistic MD simulations, including the total (solid lines) and respective cation−anion (dashed and dotted lines) profiles. The inset in both panels B and C depict schematically the cation−anion alternating stacking of the RTIL near the charged interface.

XR data for the [bmim$^+$][Tf$_2$N$^-$]/mica interfacial system is shown in Figure 4A. A similar structural model to that used for uncharged graphene was applied to the mica system (see Supporting Information for details). In this case, we found it necessary to create separate distorted layered models for the cation and the anion profiles for modeling the XR data. This accounts for the possible alternating cation/anions RTIL layers in response to surface static charges.[17] The derived best-fit electron density profile of [bmim$^+$][Tf$_2$N$^-$] at the charged mica interface is shown in Figure 4B. The origin corresponds to the average height of the oxygen atoms in the top surface. We found that including the adsorbed potassium in the model reduces the goodness of fit by almost 40%, but that quantitatively better fits to the data can be obtained when it is removed. This indicates that the potassium desorbs from the surface. The interfacial layering of adsorbed [bmim$^+$][Tf$_2$N$^-$] is pronounced in the derived profiles. These density oscillations extend as far as ~35 Å from the mica surface, significantly

farther than that for the uncharged graphene surface. This suggests that the interfacial RTIL structures are highly sensitive to the substrate surface charge, specifically leading to an extended layering of the RTIL composition. The density profile obtained from our MD simulation, employing similar empirical force fields as that used in the uncharged case (without the modifications associated with the MD II result in Figure 3) is in a very good agreement with the experimental observations. The similarity of the cation and anion density profiles between the computational and X-ray results (shown in Figure 4B,C) is striking, and highlights the alternating double-layer stacking of ion layers adjacent to the charged mica surface. Together with most recent X-ray measurements and MD simulations on various forms of RTILs,[6,17,18,57] our finding confirms that extended layering triggered by surface charges is indeed an important feature of the RTIL behavior at charged interfaces. Note also that the experimentally obtained density enhancement of the first RTIL layer (mainly cations) is only slightly greater than what MD simulations using the unmodified cross interaction parameters predict, as compared to the behavior of [bmim$^+$][Tf$_2$N$^-$] on uncharged graphene. This contrast is understood by the observation that the mica surface has no delocalized π-electron and is insulating. This further supports our conclusions that the discrepancy in the MD simulation using conventional force-fields for the graphene system is associated with the presence of an image force and π-stacking interaction which are not significant contributions to the RTIL-mica interactions.

The present results provide new insights into the interfacial ion charge distribution of ionic liquids including the observation of charge overscreening. This can be quantified from the XR determined electron density profiles since the contributions of cation and anion species have been separated in our structural analysis, as shown in Figure 5A. Here, we assume that the charge distribution is proportional to the anion/cation distributions (*i.e.*, there are no additional ionic components in the system). This result reveals significant modulations in the net charge density profile σ_p in Figure 5A, consistent with the alternating ion stacking in the RTIL. Moreover, as shown in Figure 5B, the integrated charged density normalized to the muscovite's surface charge magnitude, $\sigma_{int,n}$, as a function of height (z) from the surface unambiguously reveals the existence of charge overscreening of the RTIL at the charged interface.[58] Here, $\sigma_{int,n}(z)$ is defined as

$$\sigma_{\mathrm{int,n}}(z) = \frac{1}{\sigma_o}\int_0^z \sigma_p(z)\,dz$$

where σ_o is the negative charge density at the mica surface ($\sigma_o \approx -32\ \mu$C/cm^2).[52] Quantitatively, the respective normalized charge density per unit surface area can be obtained by sorting the volume density into monolayer bins having the width of the molecular size of the RTIL along the surface normal, as illustrated

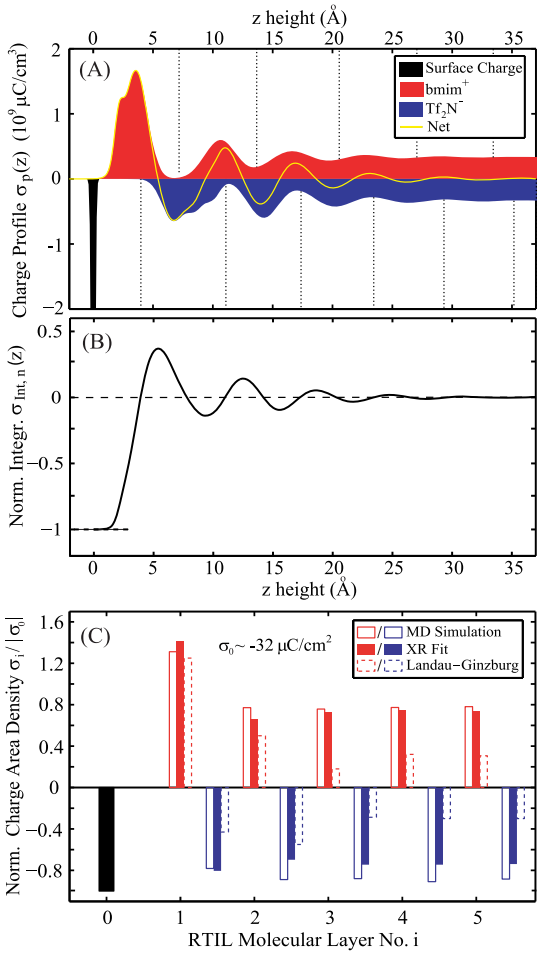

Figure 5. Charge density profiles within [bmim$^+$][Tf$_2$N$^-$] molecules as a function of heights above the charged mica surface with a charge density $\approx -32\ \mu$C/cm^2. (A) Charge density profiles σ_p (z) of the cations and anions, along with the net charge *versus* z height, as obtained from XR determined electron density profiles. (B) The integrated charged density $\sigma_{int,n}$ (z) normalized to that of the mica surface charge as a function z height. (C) Vertical distribution of the normalized charge density distribution of cations (solid bars) and anions (empty bars) sorted into RTIL monolayer bins. The XR determined result is compared with predictions by MD simulations and a simple Landau−Ginzburg-type continuum theory.

in Figure 5C. The cation and anion groups in the RTIL adjacent to the charged surface tend to stack layer-by-layer with a preferentially lying down orientation,[17] thus the separation of molecule layers along the surface normal direction for [bmim$^+$][Tf$_2$N$^-$] is ~7 Å. These results, shown in Figure 5C, reveal that the first layer (mostly cations) closest to the negatively charged surface overcompensates the mica surface charge by 41%. This charge imbalance extends out to the third layer, with a net negative charge imbalance of 5−10% of the surface charge. This effect is due to the charge overscreening at the first monolayer, implying a strong ion−ion coupling in the system. This charge overscreening phenomenon was further corroborated by our MD simulations. It is important to note that in Figure 5C the normalized charge density profile from

the MD results follows quantitatively the same trend as that observed from the X-ray measurements.

A simple phenomenological continuum theory incorporating a Landau–Ginzburg-like function for the total free energy was developed recently by Bazant *et al.* to predict analytically the interfacial structures of generic ionic liquids at charged surfaces.[30] This refined mean-field theory captures charge overscreening from short-range ion–ion correlations and lattice saturation from steric constraints of finite sizes of ions. In this model, one of the most critical physical quantities is the dimensionless correlation length, which is the ratio of the physical correlation length (l_c) and the Debye length (λ_D). Usually, l_c is in the order of the ion size (a), and λ_D is very close to 1 Å for most ionic liquids. Therefore, the ion size becomes the most relevant length scale. In their work, an ion size of 10 Å was used in the analysis of the modified Poisson-Fermi equation to predict the charge profiles of an ionic liquid layer by layer. Taking into account the smaller size (~7 Å) of [bmim$^+$][Tf$_2$N$^-$] in our work, we can obtain the analytic charge density profile of our RTIL system. The charge profile for [bmim$^+$][Tf$_2$N$^-$] at the mica surface with a charge density $\sigma = -32\ \mu C/cm^2$ is similar to that found for a generic ionic liquid, whose cation–anion charge profiles were shown in Figure 3 in the work of Bazant *et al.* for a surface charged density of $|\sigma| = 16\ \mu C/cm^2$.[30] This point stresses the expected sensitivity of an RTIL interfacial structure at a charged interface to steric constraints, including the ion size.[59] As shown in Figure 5C, the analytic prediction of this model is in good agreement with the XR and MD results for the first counterion layer close to the charged surface. However, it overestimates the charge imbalance in the third layer, as compared to the XR and MD results. In fact, this discrepancy has been noted in the work of Bazant *et al.*[30] when their analytic prediction for $|\sigma| = 16\ \mu C/cm^2$ was compared with their own MD simulation in a previous work.[60] Our results confirm that the simple phenomenological theory provides a *qualitative* description of RTIL layering and charge overcompensation at highly charged interfaces, but does not provide a fully quantitative description of this boundary behavior even though it incorporated the strong ion–ion correlations found in ionic liquids. Additional theoretical efforts are needed, especially, to capture the steric effects due to the shape and conformation of the particular RTIL and to incorporate more sophisticated models for short-range correlations,[27,61,62] through the integration with molecular-scale structural refinements and parallel atomistic MD simulations.

CONCLUSIONS

Our study provides the first molecular-scale insight into the layering of an RTIL at charged and uncharged solid surfaces through direct *in situ* observations coupled with atomistic simulations. We have developed a fundamental understanding of the molecular-level structures and intrinsic interactions of the interfacial RTIL structure. The combined high resolution X-ray interface scattering and fully atomistic MD simulations show us an enhanced interfacial densification of the first adsorbed liquid layer of the RTIL at uncharged graphene, and an alternating cation–anion double-layer stacking formation of the RTIL adjacent to charged mica. The underestimation of the density enhancement of [bmim$^+$][Tf$_2$N$^-$] at the uncharged graphene surface by simulations could be attributed to image charge effects and π–π stacking interactions not explicitly accounted for between the RTIL and the graphene basal plane; however, both of these effects would increase graphene–RTIL interactions. Through a simple modification of the existing force field to increase graphene–RTIL attraction, we were able to account for the experimentally observed interfacial electron density. The observation of pronounced charge overscreening of the RTIL at the mica surface highlights the critical role of short-range Coulomb-induced correlations on RTIL properties at a charged interface. Our experiments and simulations provide the first test of the validity of analytical predictions on charge overscreening within the framework of a Landau–Ginzburg-type continuum theory incorporating ion correlation effects. The physical insights revealed lay a foundation for understanding the RTIL structure at electrified graphene surfaces (having an externally applied potential rather than static surface charges) *via* our integrated experimental–simulation–modeling approach which is fundamental to understand and control the interactions of similar electrolytes at electrode surfaces in electrochemical energy storage systems.

METHODS

Epitaxial Graphene Growth and Characterization. Epitaxial graphene (EG) film was grown on on-axis cut 6H-SiC (0001) wafer (nitrogen doped; Cree Inc., USA) by thermal decomposition in a vacuum oven (Solar Atmospheres, PA) at 1200–1500 °C in a high vacuum of 10^{-6} Torr (heating rate: 10 K/min). EG samples were characterized by both Raman spectroscopy and atomic force microscopy (AFM). Raman spectra were recorded with an inVia Renishaw (Gloucestershire, UK) microRaman-spectrometer. An Ar-ion laser with horizontal polarization was operated at 514.5 nm in a backscattering geometry. The spectral resolution was 1.7 cm^{-1} (1800 lines/mm grating) and the lateral resolution was 0.7 μm. Surface morphology of EG was measured in tapping mode using a multimode, Digital Instruments Nanoscope IIIa AFM in air at room temperature.

Preparation of Mica Substrate. A gem-quality single crystal of muscovite (from Asheville Schoonmaker Mica Company; 25 mm × 25 mm × 0.2 mm) was cleaved to expose a fresh (001) cleavage surface and immediately rinsed by deionized water, and then immersed in a 50 mL centrifuge tube containing deionized water

for more than 1 h. Then, it was taken out, dried out, and transferred to a thin-film sample cell filled with the ionic liquid for the X-ray reflectivity measurements.

Preparation of [bmim$^+$][Tf2N$^-$] Ionic Liquid. High quality room temperature ionic liquid 1-butyl-3-methylimidazolium bis-(trifluoromethanesulfonyl), abbreviated as [bmim$^+$][Tf$_2$N$^-$], was synthesized by a method described in ref 63. Large quantity, odorless, and colorless, spectroscopic grade [bmim$^+$][Tf$_2$N$^-$] liquid was obtained to avoid chemical impurities that might complicate the interpretation of the X-ray data. The sensitivity of the liquid to synchrotron radiation damage was also tested. No significant radiation induced effects, that is, change in reflectivity at a fixed momentum transfer with time, were observed within 1 h of continuous X-ray illumination at an undulator beamline with a typical flux of around 10^{12} photons/s.

Interfacial Structure Probed Using High Resolution X-ray Reflectivity. The ionic liquid-substrate interface was probed by measuring the specular X-ray reflectivity (XR) signal at the 6-ID and 33-ID beamlines of the Advanced Photon Source. A thin film sample cell and a Roper CCD X-ray detector were mounted on a six-circle goniometer (a Huber psi-C diffractometer at 6-ID and a Newport Kappa diffractometer at 33-ID). The incidence beam, usually defined by a pair of slits [0.05−0.4 mm (vertical) × 0.5−2 mm (horizontal)], was reflected from the sample. The specular crystal truncation rod was recorded as a function of vertical momentum transfer, $Q = (4\pi/\lambda)\sin(2\theta/2)$ (where λ is the X-ray wavelength 0.9501 Å and 2θ is the scattering angle). This is also written in terms of the substrate reciprocal lattice index L in reciprocal lattice units (r.l.u.) as $L = Qc/2\pi$, where c is the vertical lattice spacing of the substrate. Application of XR techniques to liquid/solid systems and measurement procedures are described in detail in previous publications.[24]

Fully Atomistic Molecular Dynamics Simulations. To model the RTIL at epitaxial graphene surface, fully atomistic molecular dynamics (MD) simulations of [bmim$^+$][Tf$_2$N$^-$] at a graphene interface (consisting of three layers of flexible graphene sheets) were run to get a better understanding of the interfacial behavior of the ionic liquid. The modeled system consisted of 384 ion pairs and three graphene sheets, each made up of 1188 carbon atoms with a surface area of 6.64 × 4.69 nm^2. The ionic liquid was modeled using a fully atomistic flexible force field parametrized to reproduce experimentally measured values of its properties, for example, density, isobaric expansivity, isothermal compressibility, and self-diffusion coefficient.[43] The graphene sheets were represented by the AIREBO potential,[64] which results in a realistic flexible model for graphene, to ensure that the structure of the liquid is not influenced by artifacts caused by the use of a rigid mode for graphene. The simulations were performed in the canonical NVT (fixed molecule number N, fixed volume V, and fixed temperature T) ensemble using the LAMMPS[65] package with a time step of 1 fs, a general intermolecular interaction cutoff of 12 Å, and a Nosé−Hoover thermostat with $T = 298$ K. To rule out the influence of confinement on the results, the interfacial system was run in a slab geometry, which means it was periodic in two dimensions parallel to the electrode surface. The long-range interactions were handled by a 2D-modification of the particle−particle particle−mesh (PPPM) method, as implemented in LAMMPS, ensuring that no unwanted slab−slab interactions occur. All simulations were equilibrated for several (∼3 to 5) nanoseconds, followed by production runs of over a similar period of time to ensure proper sampling. The IL−graphene interactions were modeled by a simple Lennard-Jones interaction with parameters obtained by the Lorentz−Berthelot combining rules from the IL−IL and graphene−graphene interactions. Lorentz−Berthelot combining rules are commonly employed when no fitted cross-interaction parameters are available. In the Lorentz−Berthelot combining rules, the zero point of the van der Waals interaction between unlike atoms is given by $\sigma_{ij} = (\sigma_i + \sigma_j)/2$ and the well depth of the attraction by $\varepsilon_{ij} = (\varepsilon_i\varepsilon_j)$, where σ_α and ε_α are respectively the zero point and well depth of the van der Waals interaction between atoms of type $\alpha = i,j$.

To accurately capture the behavior of [bmim$^+$][Tf$_2$N$^-$] at a charged mica surface, we performed molecular dynamics simulations using the most atomistically detailed and fully flexible models available, that is, the model of Heinz *et al.*[66] for the mica surface and the all-atom model of Zhao *et al.*[43] for the ionic liquid. In all cases interaction potentials were truncated at 15 Å, with standard tail corrections added, and electrostatic interactions were accounted for using the PPPM technique. Finally, interactions between the [bmim$^+$][Tf$_2$N$^-$] ions and the mica surface were obtained using the Lorentz−Berthelot combining rules. The simulated system initially consisted of 1000 ion pairs with a random spatial distribution in contact with the surface of a block of mica composed of four mica sheets with a surface area of approximately 8 × 8 nm^2. The surface of the mica sheet was then charged by removing the neutralizing K$^+$ cations from the exposed surface, with an additional 270 [bmim$^+$] ions in order to maintain the overall neutrality of the system. Following this, electron densities were then calculated *via* a 4 ns simulation with approximately the first 2 ns being discarded for equilibration of the system and the remaining approximately 2 ns used for data gathering.

Conflict of Interest: The authors declare no competing financial interest.

Acknowledgment. We thank especially Professor G. A. Baker at the Department of Chemistry in University of Missouri-Columbia for helping the synthesis of high purity [bmim$^+$][Tf$_2$N$^-$]. This material is based upon work supported as part of the Fluid Interface Reactions, Structures and Transport (FIRST) Center, an Energy Frontier Research Center funded by the U.S. Department of Energy (DOE), Office of Science (SC), Office of Basic Energy Sciences (BES). Use of the beamlines 6ID and 33ID at the Advanced Photon Source was supported by DOE-SC-BES under Contract DE-AC02-06CH11357 to UChicago Argonne, LLC as operator of Argonne National Laboratory. This research used resources of the National Energy Research Scientific Computing Center, which is supported by DOE-SC under Contract No. DE-AC02-05CH11231, and the Palmetto cluster at Clemson University. V. Presser acknowledges financial support by the Alexander von Humboldt Foundation.

Supporting Information Available: Details of analytic methods for analysis of X-ray reflectivity data and details of important parameters of interests from structural refinements. This material is available free of charge *via* the Internet at http://pubs.acs.org.

REFERENCES AND NOTES

1. Armand, M.; Endres, F.; MacFarlane, D. R.; Ohno, H.; Scrosati, B. Ionic-Liquid Materials for the Electrochemical Challenges of the Future. *Nat. Mater.* **2009**, *8*, 621–629.
2. Simon, P; Gogotsi, Y. Materials for Electrochemical Capacitors. *Nat. Mater.* **2008**, *7*, 845–854.
3. Marsh, K. N; Boxall, J. A.; Lichtenthaler, R. Room Temperature Ionic Liquids and Their Mixtures—A Review. *Fluid Phase Equilib.* **2004**, *219*, 93–98.
4. Wishart, J. F. Energy Applications of Ionic Liquids. *Energy Environ. Sci.* **2009**, *2*, 956–961.
5. Baldelli, S. Surface Structure at the Ionic Liquid−Electrified Metal Interface. *Acc. Chem. Res.* **2008**, *41*, 421–431.
6. Kislenko, S. A.; Samoylov, I. S.; Amirov, R. H. Molecular Dynamics Simulation of the Electrochemical Interface between a Graphite Surface and the Ionic Liquid [BMIM][PF$_6$]. *Phys. Chem. Chem. Phys.* **2009**, *11*, 5584–5590.
7. Wang, S.; Li, S.; Cao, Z.; Yan, T. Y. Molecular Dynamic Simulations of Ionic Liquids at Graphite Surface. *J. Phys. Chem. C* **2010**, *114*, 990–995.
8. Vatamanu, J.; Borodin, O.; Smith, G. D. Molecular Insights into the Potential and Temperature Dependences of the Differential Capacitance of a Room-Temperature Ionic Liquid at Graphite Electrodes. *J. Am. Chem. Soc.* **2010**, *132*, 14825–14833.
9. Wu, P.; Huang, J. S.; V; Meunier, V.; Sumpter, B. G.; Qiao, R. Complex Capacitance Scaling in Ionic Liquids-Filled Nanopores. *ACS Nano* **2011**, *5*, 9044–9051.
10. Wang, J. Y.; Chu, H. B.; Li, Y. Why Single-Walled Carbon Nanotubes Can Be Dispersed in Imidazolium-Based Ionic Liquids. *ACS Nano* **2008**, *2*, 2540–2546.

11. Shim, Y. S.; Kim, H. J. Solvation of Carbon Nanotubes in a Room-Temperature Ionic Liquid. *ACS Nano* **2009**, *3*, 1693–1702.
12. Shim, Y. S.; Kim, H. J. Nanoporous Carbon Supercapacitors in an Ionic Liquid: A Computer Simulation Study. *ACS Nano* **2010**, *4*, 2345–2355.
13. Ganesh, P.; Kent, P. R. C.; Mochalin, V. Formation, Characterization, and Dynamics of Onion-like Carbon Structures for Electrical Energy Storage from Nanodiamonds Using Reactive Force Fields. *J. Appl. Phys.* **2011**, *110*, 073506.
14. Kim, T. Y.; Lee, H. W.; Stoller, M.; Dreyer, D. R.; Bielawski, C. W.; Ruoff, R. S.; Suh, K. S. High-Performance Supercapacitors Based on Poly(ionic liquid)-Modified Graphene Electrodes. *ACS Nano* **2011**, *5*, 436–442.
15. Zhao, X.; Zhang, L. L.; Murali, S.; Stoller, M. D.; Zhang, Q. H.; Zhu, Y. W.; Ruoff, R. S. Incorporation of Manganese Dioxide within Ultraporous Activated Graphene for High-Performance Electrochemical Capacitors. *ACS Nano* **2012**, *6*, 5404–5412.
16. Kamat, P. V. Graphene-Based Nanoassemblies for Energy Conversion. *J. Phys. Chem. Lett.* **2011**, *2*, 242–251.
17. Mezger, M.; Schroeder, H.; Reichert, H.; Schramm, S.; Okasinski, J. S.; Schroeder, S.; Honkimaki, V.; Deutsch, M.; Ocko, B. M.; Ralston, J.; *et al.* Molecular Layering of Fluorinated Ionic Liquids at a Charged Sapphire (0001). *Surf. Sci.* **2008**, *322*, 424–428.
18. Mezger, M.; Schramm, S.; Schroeder, H.; Reichert, H.; Deutsch, M.; De Souza, E. J.; Okasinski, J. S.; Ocko, B. M.; Honkimaki, V.; Dosch, H. Layering of $[BMIM]^+$-Based Ionic Liquids at a Charged Sapphire Interface. *J. Chem. Phys.* **2009**, *131*, 094701.
19. Korenblit, Y.; Rose, M.; Kockrick, E.; Borchardt, L.; Kvit, A.; Kaskel, S.; Yushin, G. High-Rate Electrochemical Capacitors Based on Ordered Mesoporous Silicon Carbide-Derived Carbon. *ACS Nano* **2010**, *4*, 1337–1344.
20. Pech, D.; Brunet, M.; Durou, H.; Huang, P.; Mochalin, V.; Gogotsi, Y.; Taberna, P. L.; Simon, P. Ultrahigh-Power Micrometre-Sized Supercapacitors Based on Onion-like Carbon. *Nat. Nanotechnol.* **2010**, *5*, 651–654.
21. Wu, Z. S.; Ren, W. C.; Xu, L.; Li, F.; Cheng., H. M. Doped Graphene Sheets as Anode Materials with Superhigh Rate and Large Capacity for Lithium Ion Batteries. *ACS Nano* **2011**, *5*, 5463–5471.
22. Huang, H.; Chen, W.; Chen, S.; Wee, A. T. S. Bottom-up Growth of Epitaxial Graphene on 6H-SiC(0001). *ACS Nano* **2008**, *2*, 2513–2518.
23. Presser, V.; Heon, M.; Gogotsi, Y. Carbide-Derived Carbons—From Porous Networks to Nanotubes and Graphene. *Adv. Funct. Mater.* **2011**, *21*, 810–833.
24. Zhou, H.; Ganesh, P.; Presser, V.; Wander, M. C. F.; Fenter, P.; Kent, P. R. C.; Jiang, D.; Chialvo, A. A.; McDonough, J.; Shuford, K. L.; *et al.* Understanding Controls on Interfacial Wetting at Epitaxial Graphene: Experiment and Theory. *Phys. Rev. B* **2012**, *85*, 035406.
25. Crowhurst, L.; Lancaster, N. L.; Arlandis, J. M. P.; Welton, T. Manipulating Solute Nucleophilicity with Room Temperature Ionic Liquids. *J. Am. Chem. Soc.* **2004**, *126*, 11549–11555.
26. Weingärtner, H. Understanding Ionic Liquids at the Molecular Level: Facts, Problems, and Controversies. *Angew. Chem., Int. Ed.* **2008**, *47*, 654–670.
27. Kornyshev, A. A. Double-Layer in Ionic Liquids: Paradigm Change? *J. Phys. Chem. C* **2007**, *111*, 5545–5557.
28. Bazant, M. Z.; Kilic, M. S.; Storey, B. D.; Ajdari, A. Towards an Understanding of Induced-Charge Electrokinetics at Large Applied Voltages in Concentrated Solutions. *Adv. Colloid Interface Sci.* **2009**, *152*, 48–88.
29. Kilic, M. S.; Bazant, M. Z.; Ajdari, A. Steric Effects in the Dynamics of Electrolytes at Large Applied Voltages. I. Double-Layer Charging. *Phys. Rev. E* **2007**, *75*, 021502.
30. Bazant, M. Z.; Storey, B. D.; Kornyshev, A. A. Double Layer in Ionic Liquids: Overscreening *versus* Crowding. *Phys. Rev. Lett.* **2011**, *106*, 046102.
31. Xie, X. J.; Qu, L. T.; Zhou, C.; Li, Y.; Zhu, J.; Bai, H.; Shi, G. Q.; Dai, L. M. An Asymmetrically Surface-Modified Graphene Film Electrochemical Actuator. *ACS Nano* **2010**, *4*, 6050–6054.
32. Kim, T. Y.; Lee, H. W.; Kim, J. E.; Suh, K. S. Synthesis of Phase Transferable Graphene Sheets Using Ionic Liquid Polymers. *ACS Nano* **2010**, *4*, 1612–1618.
33. Maruyama, S.; Takeyama, Y.; Taniguchi, H.; Fukumoto, H.; Itoh, M.; Kumigashira, H.; Oshima, M.; Yamamoto, T.; Matsumoto, Y. Molecular Beam Deposition of Nanoscale Ionic Liquids in Ultrahigh Vacuum. *ACS Nano* **2010**, *4*, 5946–5952.
34. Werzer, O.; Cranston, E. D.; Warr, G. G.; Atkin, R.; Rutland, M. W. Ionic Liquid Nanotribology: Mica−Silica Interactions in Ethylammonium Nitrate. *Phys. Chem. Chem. Phys.* **2012**, *14*, 5147–5152.
35. Lian, J. B.; Duan, X. C.; Ma, J. M.; Peng, P.; Kim, T.; Zheng, W. J. Hematite (α-Fe_2O_3) with Various Morphologies: Ionic Liquid-Assisted Synthesis, Formation Mechanism, and Properties. *ACS Nano* **2009**, *3*, 3749–3761.
36. Lee, D. S.; Riedl, C.; Krauss, B.; Klitzing, K. V.; Starke, U.; Smet, J. H. Raman Spectra of Epitaxial Graphene on SiC and of Epitaxial Graphene Transferred to SiO_2. *Nano Lett.* **2008**, *8*, 4320–4325.
37. Wong, S. L.; Huang, H.; Wang, Y. Z.; Cao, L.; Qi, D. C.; Santoso, I.; Chen, W.; Wee, A. T. S. Quasi-Free-Standing Epitaxial Graphene on SiC (0001) by Fluorine Intercalation from a Molecular Source. *ACS Nano* **2011**, *5*, 7662–7668.
38. Fenter, P. A.; Zhang, Z. Model-Independent One-Dimensional Imaging of Interfacial Structures at <1 Å Resolution. *Phys. Rev. B* **2005**, *72*, 081401.
39. Cheng, L.; Fenter, P. A.; Nagy, K. L.; Schlegel, M. L.; Sturchio, N. C. Molecular-Scale Density Oscillations in Water Adjacent to a Mica Surface. *Phys. Rev. Lett.* **2001**, *87*, 156103.
40. Magnussen, O. M.; Ocko, B. M.; Regan, M. J.; Penanen, K.; Pershan, P. S.; Deutsch, M. X-ray Reflectivity Measurements of Surface Layering in Liquid Mercury. *Phys. Rev. Lett.* **1995**, *74*, 4444–4447.
41. Yokota, Y.; Harada, T.; Fukui, K. Direct Observation of Layered Structures at Ionic Liquid/Solid Interfaces by Using Frequency-Modulation Atomic Force Microscopy. *Chem. Commun.* **2010**, *46*, 8627–8629.
42. Girifalco, L. A.; Hodak, M.; Lee, R. S. Carbon Nanotubes, Buckyballs, Ropes, and a Universal Graphitic Potential. *Phys. Rev. B* **2000**, *62*, 13104–13110.
43. Zhao, W.; Eslami, H.; Cavalcanti, W. L.; Muller-Plathe, F. A Refined All-Atom Model for the Ionic Liquid 1-*n*-Butyl-3-methylimidazolium Bis(trifluoromethylsulfonyl)imide [bmim][Tf_2N]. *Z. Phys. Chem.* **2007**, *221*, 1647–1662.
44. Kondrat, S.; Georgi, N.; Fedorov, M. V.; Kornyshev, A. A. A Superionic State in Nano-Porous Double-Layer Capacitors: Insights from Monte Carlo Simulations. *Phys. Chem. Chem. Phys.* **2011**, *13*, 11359–11366.
45. Kondrat, S.; Kornyshev, A. A. Superionic State in Double-Layer Capacitors with Nanoporous Electrodes. *J. Phys.: Condens. Matter* **2011**, *23*, 022201.
46. Tsuzuki, S.; Mikami, M.; Yamada, S. Origin of Attraction, Magnitude, and Directionality of Interactions in Benzene Complexes with Pyridinium Cations. *J. Am. Chem. Soc.* **2007**, *129*, 8656–8662.
47. Wang, Y. T.; Voth, G. A. Unique Spatial Heterogeneity in Ionic Liquid. *J. Am. Chem. Soc.* **2005**, *127*, 12192–12193.
48. Triolo, A.; Russina, O.; Bleif, H. J.; Cola, E. D. Nanoscale Segregation in Room Temperature Ionic Liquids. *J. Phys. Chem. B* **2007**, *111*, 4641–4644.
49. Chen, S. M.; Kobayashi, K.; Kitaura, R.; Miyata, Y.; Shinohara, H. Direct HRTEM Observation of Ultrathin Freestanding Ionic Liquid Film on Carbon Nanotube Grid. *ACS Nano* **2011**, *5*, 4902–4908.
50. Guymon, C. G.; Rowley, R. L.; Harb, J. N.; Wheeler, D. R. Simulating an Electrochemical Interface Using Charge Dynamics. *Condens. Matter Phys.* **2005**, *8*, 335–356.
51. Payne, C. M.; Zhao, X.; Vlcek, L.; Cummings, P. T. Molecular Dynamics Simulation of ss-DNA Translocation between Copper Nanoelectrodes Incorporating Electrode Charge Dynamics. *J. Phys. Chem. B* **2008**, *112*, 1712–1717.
52. Schlegel, M. L.; Nagy, K. L.; Fenter, P.; Cheng, L.; Sturchio, N. C.; Jacobsen, S. D. Cation Sorption on the Muscovite (001)

Surface in Chloride Solutions Using High-Resolution X-ray Reflectivity. *Geochim. Cosmochim. Acta* **2006**, *70*, 3549–3565.
53. Bowers, G. M.; Bish, D. L.; Kirkpatrick, R. J. Cation Exchange at the Mineral−Water Interface: pH Dependence of K^+ Displacement at the Surface of Nano-muscovite. *Langmuir* **2008**, *24*, 10240–10244.
54. Liu, Y. D.; Zhang, Y.; Wu, G. Z.; Hu, J. Coexistence of Liquid and Solid Phases of Bmim-PF_6 Ionic Liquid on Mica Surfaces at Room Temperature. *J. Am. Chem. Soc.* **2006**, *128*, 7456–7457.
55. Bovio, S.; Podesta, A.; Lenardi, C.; Milani, P. Evidence of Extended Solidlike Layering in [Bmim][NTf_2] Ionic Liquid Thin Films at Room-Temperature. *J. Phys. Chem. B* **2009**, *113*, 6600–6603.55.
56. Yokota, Y.; Harada, T.; Fukui, K. Direct Observation of Layered Structures at Ionic Liquid/Solid Interfaces by Using Frequency-Modulation Atomic Force Microscopy. *Chem. Commun.* **2010**, *46*, 8627–8629.
57. Sha, M. L.; Wu, G. Z.; Dou, Q.; Tang, Z. F.; Fang, H. P. Double-Layer Formation of [Bmim][PF_6] Ionic Liquid Triggered by Surface Negative Charge. *Langmuir* **2010**, *26*, 12667–12672.
58. Levin, Y. Electrostatic Correlations: from Plasma to Biology. *Rep. Prog. Phys.* **2002**, *65*, 1577–1632.
59. Feng, G.; Qiao, R.; Huang, J.; Dai, S.; Sumpter, B. G.; Meunier, V. The Importance of Ion Size and Electrode Curvature on Electrical Double Layers in Ionic Liquids. *Phys. Chem. Chem. Phys.* **2011**, *13*, 1152–1161.
60. Fedorov, M. V.; Kornyshev, A. A. Towards Understanding the Structure and Capacitance of Electrical Double Layer in Ionic Liquids. *Electrochim. Acta* **2008**, *53*, 6835–6840.
61. Feng, G.; Huang, J. S.; Sumpter, B. G.; Meunierc, V.; Qiao, R. A "Counter-charge Layer in Generalized Solvents" Framework for Electrical Double Layers in Neat and Hybrid Ionic Liquid Electrolytes. *Phys. Chem. Chem. Phys.* **2011**, *13*, 14723–14734.
62. Wu, J. Z.; Jiang, T.; Jiang, D. E.; Jin, Z. H.; Henderson, D. A Classical Density Functional Theory for Interfacial Layering of Ionic Liquids. *Soft Matter* **2011**, *7*, 11222–11231.
63. Burrell, A. K.; Del Sesto, R. E.; Baker, S. N.; McCleskey, T. M.; Baker, G. A. The Large Scale Synthesis of Pure Imidazolium and Pyrrolidinium Ionic Liquids. *Green Chem.* **2007**, *9*, 449–454.
64. Stuart, S. J.; Tutein, A. B.; Harrison, J. A. A Reactive Potential for Hydrocarbons with Intermolecular Interactions. *J. Chem. Phys.* **2000**, *112*, 6472–6486.
65. Plimpton, S. Fast Parallel Algorithms for Short-Range Molecular Dynamics. *J. Comput. Phys.* **1995**, *117*, 1–19.
66. Heinz, H.; Koerner, H.; Anderson, K. L.; Vaia, R. A.; Farmer, B. L. Force Field for Mica-type Silicates and Dynamics of Octadecylammonium Chains Grafted to Montmorillonite. *Chem. Mater.* **2005**, *17*, 5658–5669.